Distribution of relaxation times analysis of rotating disk electrode impedance spectra

Alexander Rampf [a], Carla Marchfelder [a,b], Roswitha Zeis [a,b,c,*]

[a] *Karlsruhe Institute of Technology, Helmholtz Institute Ulm, Helmholtzstraße 11, 89081 Ulm, Germany*
[b] *Friedrich-Alexander-Universität Erlangen-Nürnberg, Department of Electrical Engineering, 91058 Erlangen, Germany*
[c] *University of Toronto, Department of Mechanical and Industrial Engineering, 5 King's College Road, Toronto, Ontario M5S 3G8, Canada*

ARTICLE INFO

ABSTRACT

Distribution of relaxation times (DRT) is a valuable analytical tool to identify and quantify individual contributions in electrochemical impedance spectroscopy (EIS) data. This study introduces the DRT method for rotating disk electrode (RDE) measurements using the example of the oxygen reduction reaction (ORR) in alkaline media. A comprehensive peak assignment is presented based on the variation of different parameters, such as the oxygen saturation level in the electrolyte, the rotation rate, and the current density. Two prominent peaks in the low-frequency area are attributed to the oxygen mass transport and the charge transfer of the ORR. Additionally, three minor high-frequency peaks are identified. This assignment may serve as a reference for other researchers who intend to employ DRT for the RDE, regardless of the investigated reaction. Furthermore, a direct correlation between the Koutecký-Levich evaluation and the DRT analysis is demonstrated, indicating that DRT can be used similarly to the Koutecký-Levich analysis to extract kinetic information. This enables the possibility of performing and evaluating long-term in-situ steady-state measurements where the conventional Koutecký-Levich analysis is not applicable.

1. Introduction

Distribution of Relaxation Times (DRT) analysis is a tool for evaluating electrochemical impedance spectroscopy (EIS) data. In recent years, there has been a notable increase in the number of publications on this topic [1]. DRT analysis has been employed in a variety of studies, spanning different fields like low-temperature [2,3] and high-temperature polymer electrolyte membrane fuel cells (PEMFC) [4, 5], electrochemical hydrogen pumps [6], electrolyzers [7], and diverse battery types [1,8–10].

DRT analysis is a complementary method to equivalent circuit modeling. The advantage of this approach is that no a priori knowledge of the system is required [11,12]. The DRT model consists of a series of RC elements and a single ohmic resistance and can be expressed as a linear mathematical equation [13]. When applied to EIS data, the equation can be solved by software based on the relatively straightforward quadratic optimization problem in a few milliseconds [14]. However, a regularization method is required since calculating the DRT from experimental data is an ill-posed problem [15]. The regularization parameter is a crucial parameter for the DRT and should be chosen as

small as possible to achieve a high resolution and as high as required to avoid false peaks [16]. The result of a DRT transformation is a so-called DRT plot, which visualizes single processes as peaks in the corresponding time domains. In this plot, each peak corresponds to a specific physicochemical process occurring within the investigated system. The y-axis $g(f)$ describes the impedance distribution over the respective frequency. The position of each peak represents the time scale of the process, while the peak area corresponds to the impedance of the process. The processes associated with each peak are unknown in a system where DRT analysis is employed for the first time. A typical approach to identify the corresponding processes is to modify individual parameters and observe the impact on the peaks in the DRT plot [4].

In this work, we introduce the application of the DRT analysis to the rotating disk electrode (RDE). The RDE is a versatile and widely utilized method to study a catalyst's activity and durability [17,18]. One of the major fields of investigation is the study of catalysts for the oxygen reduction reaction (ORR) [19–21]. However, the RDE is also used for the analysis of catalysts for many other reactions, including the hydrogen oxidation [22,23] and evolution reaction [24], the oxygen evolution reaction [25], and the CO_2 reduction reaction [26]. This study

introduces EIS in combination with DRT analysis for the RDE by examining the ORR in alkaline media. Its objective is to serve as a guideline for other researchers who may want to implement DRT in their own RDE-based studies.

RDE data, which are mathematically described by the Koutecký-Levich equation, can typically be subdivided into three potential regions: a kinetic, a mixed, and a mass transport-controlled region [27, 28]. These regions are also observed with the DRT method. Consequently, the presented results and the general peak assignment can be transferred and used as a basis for other RDE-based studies, even for reactions other than the ORR. Moreover, we demonstrate how the DRT tool can be employed as an evaluation method for extracting kinetic information similar to the typical KL analysis. This makes DRT analysis particularly interesting for experiments where the KL requirements do not apply.

2. Experimental

The RDE measurements were conducted with a polycrystalline Pt disk electrode in 0.1 M KOH at 20 °C. The electrolyte was prepared by dissolving KOH pellets (Emplura®, Merck) in ultrapure water (0.055 μS) from the water dispenser PURELAB®flex (Elga). For the RDE measurements, the Pine E3-series Pt disk electrode (0.196 cm^2) was used in combination with the Research MSR Rotator (Pine Research Instrumentation). The reversible hydrogen electrode (RHE) HydroFlex (Gaskatel) was employed as the reference electrode (RE), while a platinized platinum plate served as the counter electrode. The electrochemical cell used in this work is made of polypropylene with an inner volume of 250 ml. It is closed at the top by a screw cap, which contains customized openings for the respective electrodes and the gas tube, to minimize the influence of the surrounding gas atmosphere. Nitrogen or oxygen was purged into the electrolyte using a PTFE gas frit (pore size: 5 μm, Bohlender) 30 min before starting the measurement to guarantee a complete gas saturation of the respective gas. All electrochemical measurements were conducted on a Zennium potentiostat (Zahner Elektrik).

Before each experiment, the Pt disk electrode was polished with alumina slurry (0.05 mm, Buehler) on various Buehler polishing pads to achieve a mirror-smooth surface. It was then thoroughly washed and placed in an ultrasonic bath for 5 min.

Prior to the measurements in the oxygen-saturated electrolyte, a typical Pt pre-treatment was performed in the oxygen-free electrolyte. To achieve steady-state voltammograms, 30 cyclic voltammetry (CV) scans were recorded between 0.05–1.10 V at 50 mV s^{-1}. Subsequently, the electrolyte was purged with oxygen. Electrochemical impedance spectroscopy (EIS) measurements were performed in a specific sequence beginning with 3 CV scans between 0.0–1.0 V at 50 mV s^{-1} to ensure identical starting conditions. This was followed by 5 min of chronopotentiometry, during which the same current density was applied as in the subsequent galvanostatic EIS measurement. The goal of this step was to reach a state of equilibrium. Finally, the actual EIS measurement was performed over the frequency range of 20 kHz to 1 Hz, with an amplitude of 10 μA, except for the measurement at 0.1 mA cm^{-2}, which was conducted with an amplitude of 5 μA. For each measurement sequence, a single parameter was varied. The parameters investigated in this study were the oxygen saturation level in the electrolyte, the rotation rate, and the current density. Additionally, a measurement over time was carried out at a constant current density of 1.0 mA cm^{-2}. The selected standard values were a rotation rate of 1600 rpm and a fully oxygen-saturated 0.1 M KOH electrolyte. All potentials in this work are given versus the RHE.

Measurements at different oxygen saturation levels were performed by using a gas flow controller (Brooks Instrument). The respective oxygen saturation value %O$_2$ was determined by the Levich Eq. (1), which consists of the following variables: the limiting current I_L, the number of transferred electrons n, the Faraday constant F, the electrode area A, the diffusion coefficient D, the angular rotation rate ω, the kinematic viscosity ν, and the concentration of the redox-active species c in the electrolyte.

$$I_L = 0.62 \, n \, F \, A \, D^{\frac{2}{3}} \, \omega^{\frac{1}{2}} \, \nu^{-\frac{1}{6}} \, c \tag{1}$$

Except for the oxygen concentration c in the electrolyte, all parameters remained constant throughout the measurement. Consequently, the oxygen saturation level was calculated by dividing the respective limiting current I_L by the limiting current in a fully saturated electrolyte $I_{L,sat}$, as illustrated in Eq. (2).

$$\%O_2 = \frac{c}{c_{sat}} \cdot 100\% = \frac{I_L}{I_{L,sat}} \cdot 100\% \tag{2}$$

The kinetic current was calculated using the Koutecký-Levich Eq. (3). The limiting current is equivalent to the mass transport current in an RDE setup.

$$j_K = \frac{j \cdot j_L}{j_L - j} \tag{3}$$

Before processing the impedance data, quality validation was performed using the Kramers-Kronig test via the LIN-KK software [29]. Selected results of the Kramers-Kronig test at boundary measurement conditions are shown in Fig. S1. In particular, impedance data measured at high current density and reduced current hold times demonstrate increased instability at lower frequencies. However, no evidence of systematic error or drift was observed. This confirms the system's stability during the EIS measurement. In addition, the weighted harmonics autocorrelation algorithm of the Zahner software was employed to determine the linearity of the impedance data. The significance was always greater than 0.990, with the majority of data points exceeding 0.999. However, a few data points from the measurements at 0.1 and 0.2 mA cm^{-2} exhibited a significance below 0.990 at low frequencies, with 0.981 being the lowest.

The DRT transformation was conducted via the software RelaxIS (version 3.0.22, rhd instruments) based on the Gaussian function for the discretization. Additionally, the peak area and the peak position were determined with this program. A regularization parameter λ of 0.0001 was chosen. To ascertain it, the sum of square residuals (SSR) between the measured impedance data and impedance spectra reconstructed from DRT was plotted against λ (see Fig. 1). A lower regularization parameter provides a better fit to the measured impedance data. However, a value that is too small may result in the generation of artificial peaks in the DRT due to measurement uncertainty [2,6]. Therefore, the value at which the SSR does not decrease further was employed as the value for the regularization parameter λ.

3. Results and discussion

This study aims to introduce the DRT analysis as an analytical tool to separate and quantify impedance-related processes for RDE-based experiments. Accordingly, this section begins with a general assignment of the peaks in the DRT spectra. This should provide an overview of how a typical Nyquist plot and the corresponding DRT spectrum appear. In the following subsections, single parameters are varied to investigate their influence on the Nyquist plot and the DRT spectrum. Furthermore, the peak assignment is discussed in detail based on the varied parameters. Finally, the DRT analysis of RDE data is compared with the classical Koutecký-Levich analysis.

3.1. General peak assignment of the DRT spectra

Fig. 2a illustrates a typical Nyquist plot based on EIS data acquired with the RDE setup. The colored semicircles are reconstructed using the time-constant information provided by the DRT analysis to visualize the single impedance contributions.

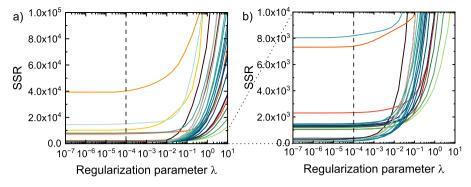The corresponding DRT plot (Fig. 2b) reveals five peaks attributed to

Fig. 1. a) The sum of square residuals (SSR) between the measured EIS data and the reconstruction from the DRT at different regularization parameters for all measurements in this work; b) enlarged visualization. Chosen regularization parameter of 10^{-4} is highlighted by a dashed line. Curves have the identical color used also later for the corresponding measurement.
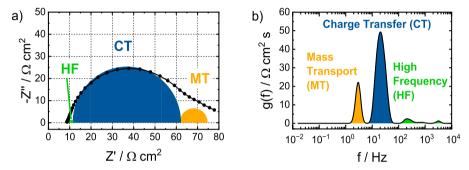

Fig. 2. a) Exemplary Nyquist plot with assigned processes taken from b) the DRT analysis. EIS measurement was conducted at 1.0 mA cm^{-2} at 1600 rpm in a fully oxygen-saturated 0.1 M KOH electrolyte.

physicochemical processes occurring within the system. The assignment was made based on the variation of single experimental parameters. The peak observed at low frequencies at around 3 Hz is assigned to the mass transport (MT) impedance of oxygen to the electrode. The peak next to it, at 20 Hz, is identified as the charge transfer (CT) impedance of the ORR. Furthermore, three minor peaks are visible at frequencies above 50

Hz, which remain unassigned to a specific process. These peaks are probably associated with one of the following processes: a fast reaction step of the ORR, hydroxide adsorption, or double-layer charging. Henceforth, these three peaks will be summarized and labeled as high-frequency peaks.

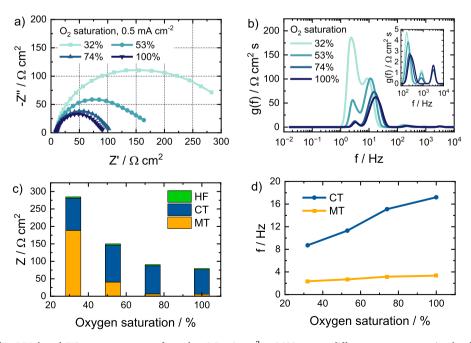This study primarily focuses on the two prominent peaks, which can

Fig. 3. a) Nyquist plot of Pt-RDE based EIS measurements performed at 0.5 mA cm^{-2} at 1600 rpm at different oxygen saturation levels in 0.1 M KOH; b) corresponding DRT plot; c) impedance contributions, and d) frequencies determined from the DRT analysis.

be unambiguously attributed and account for over 95% of the total impedance observed in all experiments. The color code illustrated in Fig. 2 will be employed throughout this work.

The general assignment of the DRT peaks applies not only to ORR-based reactions but also to all other studies conducted with RDE. The design of the RDE system dictates that the primary impedance contributions are the mass transport impedance of the redox-active species and the charge transfer impedance associated with the occurring reaction. Consequently, the assignment depicted in Fig. 2b is maintained in a general sense, without reference to a specific reaction.

3.2. Influence of the oxygen saturation level

The first parameter being investigated is the oxygen saturation level in the electrolyte. The Nyquist plot in Fig. 3a indicates a significant impedance decrease with increasing oxygen saturation in the electrolyte. The real part impedance at the high-frequency intercept with the x-axis corresponds to the ohmic resistance of the electrolyte between the working electrode (WE) and the RE and is not displayed in the DRT. In principle, it also consists of the ohmic resistances of the cables and the WE, but these contributions can be neglected [30]. The electrodes are fixed in our setup, and the temperature is kept constant. Thus, all experiments' electrolyte resistance is identical and measures 8.72 ± 0.05 Ω cm^2.

As illustrated in Fig. 3b, the corresponding DRT plots exhibit two prominent peaks. The peak at about 3 Hz decreases sharply with increasing oxygen content. Therefore, it most likely correlates with oxygen's mass transport (MT) to the electrode. Furthermore, in other DRT studies, the frequency range of 1–10 Hz has been correlated with mass transport processes in many different systems, including low-temperature and high-temperature polymer electrolyte membrane fuel cells (PEMFCs) [2,4], electrochemical hydrogen pumps (EHPs) [6], and even vanadium redox flow batteries (VRFBs) [8]. The impedance and the characteristic frequency obtained from the DRT peak are shown in Fig. 3c and d. As the DRT plot shows, the MT impedance decreases significantly until an oxygen saturation level of 74% is reached. Between 74% and 100% oxygen saturation, the MT impedance declines only by 14%. The minor reduction may be attributed to the moderate applied current density of 0.5 mA cm^{-2}, which does not consume significant oxygen, thereby preventing an oxygen deficiency near the electrode. It can be assumed that the oxygen supply is already sufficient to maintain a constant oxygen saturation at the electrode. Notably, the characteristic frequency of the MT of oxygen remains almost unaffected, exhibiting only a slight increase from 2.35 Hz to 3.34 Hz across the entire oxygen saturation range. The frequency reflects the velocity or rate of the oxygen MT to the electrode. As all measurements at varying saturation levels are conducted at an identical rotation rate of 1600 rpm, the velocity of the oxygen MT is only minimally influenced.

The peak next to the MT peak does not display such a clear trend in the DRT (Fig. 3b). The process is more rapid than the MT. In other studies, peaks in this frequency range of 10–100 Hz have been shown to correlate with the charge transfer (CT) of the ORR [2,4,5,31]. Therefore, it is presumably connected to the CT of the ORR. Another reason is that the ORR is the primary process occurring in this setup. The peak height diminishes with elevated oxygen concentration; however, a precise impedance quantification of that process can only be achieved by integrating the peak area, summarized in Fig. 3c. Indeed, the CT impedance remains relatively constant when the oxygen saturation is altered. The decline is not uniform across the entire range, with a total reduction of only 23%. Although the onset potential shifts slightly to higher potentials with an increase in oxygen concentration (see Fig. S2), which is also predicted by the Nernst equation, the reaction barrier remains relatively constant since the measurements were taken in galvanostatic rather than potentiostatic conditions. However, the corresponding CT frequency in Fig. 3d increases significantly from 8.7 Hz to 17.2 Hz. The observed increase in the CT rate can only be attributed to the elevated oxygen

content in the electrolyte, which accelerates the CT process of the ORR.

At last, three minor high-frequency peaks can be seen in the DRT plot (Fig. 3b). The peak adjacent to the CT peak shifts linearly from 155 Hz to 241 Hz with a reduction in impedance from 2.79 Ω cm^2 to 2.15 Ω cm^2. This peak, therefore, exhibits a similar behavior to that of the CT peak and can be attributed to the ORR process. It may represent a rapid step of the ORR, such as the oxygen adsorption on platinum or a proton transfer step to form the final product. Two ORR-related peaks have also been identified in the DRT plots of HT-PEMFC [4]. At around 800 Hz a further peak is observable, exhibiting the smallest peak. It disappears at 100% oxygen saturation, presumably due to the convolution with the preceding peak. It is not clear which specific process it may be attributed to. One potential assignment is hydroxide adsorption, which takes place on Pt in alkaline conditions [32,33]. The final peak is consistently observed at 3177 Hz and can be attributed to the double-layer charging. This process is known to occur rapidly and has already been reported to take place in the time domain at frequencies between 10^3 Hz and 10^4 Hz [34]. However, time domains can differ significantly when processes are examined at the macroscopic level, as is the case here, or at the considerably faster atomic level [35].

The combined impedance contribution of the three high-frequency peaks to the total impedance is <4%. Consequently, they can be considered a minor role in optimizing the ORR efficiency.

3.3. Influence of the rotation rate

The following parameter studied is the rotation rate. As the rotation rate increases, the Nyquist plot displays an increasing semicircle (Fig. 4a). The corresponding DRT plot in Fig. 4b provides insights into the impedance contributions. Four distinct peaks are identified in all experiments. The characteristic MT peak at low frequencies shifts to higher frequencies with increasing rotation rate, from 1.72 Hz to 3.94 Hz (see Fig. 4d). An increase in rotation rate results in faster oxygen transport towards the electrode. The impact of the rotation rate on the MT frequency is significantly greater than the impact of the oxygen saturation levels observed in the experiments in Fig. 3. Furthermore, a reduction of the MT impedance with increasing rotation rate is visible in Fig. 4c. This observation can be attributed to the elevated local oxygen concentration in the vicinity of the electrode at higher rotation rates. Nevertheless, the decrease is relatively minor compared to the experiments at varied oxygen saturation levels since the electrolyte in the present case is already fully oxygen-saturated. Therefore, it can be concluded that the rotation rate affects only the local oxygen concentration at the electrode.

The most prominent peak, which is correlated to the CT of the ORR, shows an inverse trend compared to the MT (Fig. 4b). A constant increase in impedance is observed, accompanied by a linear decrease in the corresponding characteristic frequency with increasing rotation rates (see Fig. 4c and d). One explanation for this phenomenon is that the oxygen transport to the electrode is accelerated at higher rotation rates. However, concurrently, oxygen is also more rapidly removed from the electrode. This reduces the probability of oxygen adsorption on the electrode and the subsequent reaction to the hydroxide. In addition, oxygen may partially react to peroxide first, followed by a reduction to hydroxide. At higher rotation rates, the detachment of the formed peroxide is more pronounced due to the elevated shear forces [36]. The increase in the incomplete reaction to peroxide at higher rotation rates can also be responsible for the increasing charge transfer impedance and its decreasing frequency.

An opposite behavior was observed by Singh et al. [37], who analyzed a thin-film catalyst layer of Pt/C on an RDE in conjunction with EIS in the potentiostatic mode at varying rotation rates in 0.1 M HClO$_4$. The authors observed that the Nyquist plot exhibits smaller semicircles with increasing rotation rates. However, the impedances are generally higher than those reported here, and the authors attributed the majority of the impedance to the external mass transport of oxygen. Additional
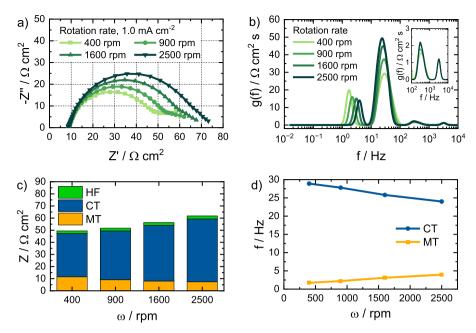
Fig. 4. a) Nyquist plot of Pt-RDE based EIS measurements performed at 1.0 mA cm^{-2} at different rotation rates in a fully oxygen-saturated 0.1 M KOH electrolyte; b) corresponding DRT plot; c) impedance contributions, and d) frequencies determined from the DRT analysis.

transport processes occurring within the catalyst layer can presumably account for their significantly higher MT impedance. To determine the impedance contributions, they assumed a constant CT impedance. However, the DRT approach in our work demonstrates that the CT impedance is not entirely rotation rate independent.

Two additional peaks in the high-frequency region of the DRT plot can be seen for all rotation rates (Fig. 4b). The peak at approximately 300 Hz follows the same trend with regard to the impedance and frequency shift as the CT peak. This supports the former assignment as an ORR-related process. The other peak, which was previously attributed to the double layer charging, remains at 3177 Hz and is entirely unaffected by changes in rotation rate. The third peak, previously observed in the middle of both, has disappeared. The slight asynchrony shape of the 300

Hz peak suggests the convolution of the peaks.

3.4. Influence of the time

In contrast to the previous experiments, which focused on the variation of a single parameter, this subsection examines the evolution of the impedance over time at an applied current density of 1.0 mA cm^{-2}. Fig. 5a displays a series of Nyquist plots over two hours. The size of the semicircle continuously increases over time. A significant increase in impedance can be especially noticed from the first measurement to the subsequent one. A clear outlier can be identified for the Nyquist plot measured after 50 min at low frequencies. This outlier was removed before proceeding with the DRT transformation. The DRT plot (Fig. 5b)
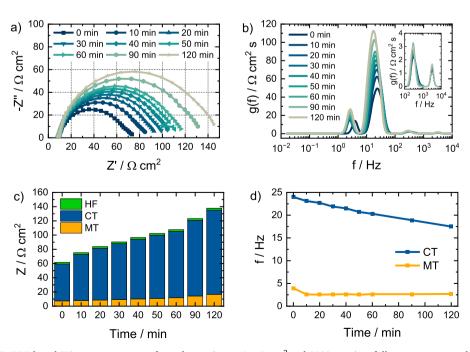

Fig. 5. a) Nyquist plot of Pt-RDE based EIS measurements performed over time at 1 mA cm^{-2} and 1600 rpm in a fully oxygen-saturated 0.1 M KOH electrolyte; b) corresponding DRT plot; c) impedance contributions, and d) frequencies determined from the DRT analysis.

reveals four peaks for each measurement.

The MT frequency declines from the first to the second measurement, decreasing from 3.94 Hz to 2.58 Hz (Fig. 5d). After that, it remains relatively stable at 2.6 Hz. We expect a constant frequency from the previous experiments since the rotation rate was kept constant, and a fully oxygen-saturated electrolyte was used. The initial decrease in frequency can only be attributed to changes at the electrode surface, which impede the oxygen MT. The potential always exceeded 0.7 V during this experiment. It is known that hydroxide adsorption usually takes place at a potential greater than 0.7 V in alkaline media [33]. Therefore, adsorbates at the electrode surface may be responsible for reducing the MT velocity to the electrode surface. This behavior could not have been observed in the experiments before since the adsorption of oxygenated species or even Pt oxidation was prevented by scanning down to low potentials before each experiment. This ensures equal and reproducible starting conditions. The corresponding MT impedance exhibits a 2.2-fold increase in the two hours of the experiment (Fig. 5c). Nevertheless, the MT impedance value of 16.6 Ω cm^{-2} after two hours of constant current is still relatively low compared to values in Fig. 3c at varied oxygen saturation levels. This suggests that the local oxygen concentration at the electrode is diminished as a consequence of the ORR. Yet, substantial oxygen quantities could be maintained due to the moderate applied current density and the constant transport of oxygen to the electrode.

The CT impedance gradually increased from 51.8 Ω cm^{-2} to 118.5 Ω cm^{-2} over the two hours. At the same time, the potential decreases from 0.79 V to 0.73 V. The reduction in catalytic activity and the increased CT impedance indicate a decrease in active sites. Like the MT frequency, this can be attributed to hydroxide adsorption and Pt oxidation over time. In the literature, it is widely accepted that the coverage of oxide species on Pt suppresses the ORR and that this coverage is described as a function of potential and time [38]. Therefore, the initial decrease in MT frequency and the increase in CT impedance can be explained by the formation of a hydroxide or an oxide layer, which is a relatively fast process. This is also indicated by the decrease in the MT frequency in <10 min. However, another mechanism, the so-called "place-exchange conversion" to PtO$_2$, which occurs after the first coverage of the Pt surface with oxide species (OH$_{ads}$ or O$_{ads}$), is a relatively slow process [39]. This process can already take place in the presence of oxygen at potentials beginning from 0.6 V [40]. Thus, this mechanism, which can lead to a reduction in the number of catalytically active sites, is responsible for the observed increase in CT impedance and decrease in potential over time. In contrast to the CT impedance, the MT frequency, which correlates with the velocity of the oxygen transport, is not affected since this is an internal conversion of the electrode surface. The corresponding CT frequency decreases during the two hours from 24.0 Hz to 17.5 Hz (Fig. 5d). As previously mentioned, the reduction in CT kinetics can be attributed to the decrease in local oxygen concentration. In addition, the coverage with adsorbates on the electrode surface also hampers the ORR kinetics.

As illustrated in Fig. 5b, the peak to the right of the CT peak in the DRT, which was correlated with a rapid sub-step of the ORR, displays a similar behavior as the CT peak. Therefore, the previous assignment can be confirmed. The highest frequency peak previously correlated with the double-layer charging remains constant at 3177 Hz and shows a slight increase over time.

3.5. Influence of the current

The next parameter under variation is the current density. The Nyquist plot in Fig. 6a displays a less clear trend. As the current density increases, the semicircle gradually diminishes in size until a current density of 1.0 mA cm^{-2} is reached. Subsequently, the curves show an increase, exhibiting a two-semicircular shape. Similar trends have been observed in several studies that have employed the RDE in conjunction with EIS [37,41–43]. The respective studies were conducted in the potentiostatic mode and predominantly in acidic electrolytes, investigating a thin-film platinum-based catalyst layer. The observed decline in impedance with decreasing potential typically continued until around 0.8 V vs. RHE, after which it increased again. The impedance values differ significantly in the aforementioned publications, which may be attributed to loading effects and the preparation of the thin film. Unfortunately, not all publications provide platinum loading information to verify this. However, the corresponding potential in our experiment at a current density of 1.0 mA cm^{-2} is 0.8 V, which confirms that both potentiostatic and galvanostatic modes provide similar results and can, therefore, be used equally. However, the galvanostatic mode used in this study facilitates a more precise comparison of the impedance
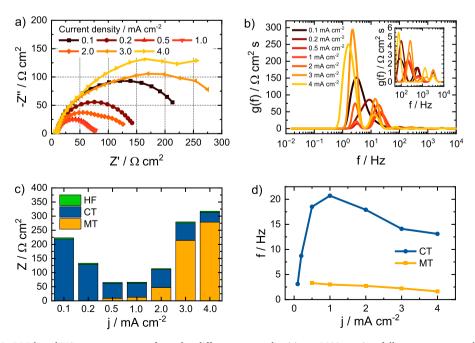

Fig. 6. a) Nyquist plot of Pt-RDE based EIS measurements performed at different current densities at 1600 rpm in a fully oxygen-saturated 0.1 M KOH electrolyte; b) corresponding DRT plot; c) impedance contributions, and d) frequencies determined from the DRT analysis.

contributions between different catalysts with varying onset potentials.

In Fig. 6b, the DRT plot shows pronounced shifts in frequencies and peak height for the prominent peaks within the MT and CT region between 1–100 Hz. The analysis starts with low current densities and then progresses to higher ones to facilitate the description. At 0.1 mA cm^{-2} with a corresponding potential of 0.86 V, a prominent peak is visible at around 3 Hz. Although the frequency range has been previously assigned to MT processes, the peak here is clearly connected with the CT impedance of the ORR. The reaction is mainly kinetically limited at such low current densities, and the mass transport has a minor influence. In the next curve at a current of 0.2 mA cm^{-2}, a clear shift in peak frequency can be seen towards higher frequencies. The shape of the peak is asynchronous, with contributions at lower frequencies. These contributions may be attributed to the MT, which is likely too small to be resolved as a separate peak. Two significant peaks emerge from the DRT curve measured at 0.5 mA cm^{-2}, corresponding to the MT and the CT. As the current density increases, the size of the MT peak increases significantly. In contrast, the CT peak does not decrease uniformly and alters its peak shape in response to the applied current.

The extraction of the specific impedance contributions and corresponding frequencies, as summarized in Fig. 6c and d, provides greater clarity. The CT impedance represents the major impedance contribution at low currents, exhibiting a 76% reduction from 0.1 mA cm^{-2} to 0.5 mA cm^{-2}, which corresponds to a potential decrease of 0.86 V to 0.82 V. This significant decline can be attributed to the increased overpotential and therefore reduced reaction/energy barriers. Upon further increasing the current, the CT impedance remains relatively constant, except in the last step, from 3.0 mA cm^{-2} to 4.0 mA cm^{-2}, which displays a significant decrease of 44% to the lowest CT impedance value of 34.4 Ω cm^2. It appears that the CT impedance, which correlates with reaction and energy barriers, does not exhibit a linear decay behavior with increasing current but rather a logarithmic one. This finding is in agreement with the description of the Tafel equation, derived from the Butler-Volmer expression, which indicates a logarithmic relationship between the current and the overpotential.

The corresponding CT frequency demonstrates a substantial increase from 3.1 Hz to 20.7 Hz at low currents (Fig. 6d), expected due to the increased overpotential and consequently accelerated reaction rate, as described in the Arrhenius equation. However, the trend reverses as the current increases above 1.0 mA cm^{-2}. This observation can be attributed to the enhanced product formation at elevated currents, which depletes the local oxygen concentration at the electrode surface, thereby reducing the CT rate.

The MT impedance cannot be quantified below 0.5 mA cm^{-2} since no single MT peak can be resolved in the DRT plot. Nevertheless, the contributions are likely smaller than those observed for the higher currents. From 0.5 mA cm^{-2} to 4.0 mA cm^{-2}, the MT impedance exhibits a >30-fold increase, while the corresponding MT frequency decreases from 3.28 Hz to 1.63 Hz (Fig. 6c and d). These results can be explained by the progressive depletion of dissolved oxygen in the direct vicinity of the electrode with increasing currents. Furthermore, the reduction in frequency may be attributed to the increased formation of products, which impede oxygen transport to the electrode, thereby reducing the oxygen MT rate.

The previously mentioned studies on RDE in conjunction with EIS have evaluated the EIS data based on either an equivalent circuit model or a thin-film/flooded agglomerate model [37,41–43]. Only one publication determines and displays the numbers of the respective impedance contributions. For a Pt/C catalyst, the authors determine a CT impedance of 5160.2 Ω cm^2 at 0.7 V vs. NHE in 0.5 M H$_2$SO$_4$ [41]. This value is significantly higher than those observed in the present work. For comparison, our study determined a CT impedance of 63 Ω cm^2 at 2 mA cm^{-2} and 0.74 V. It should be noted that the publication presented the highest impedances for Pt/C catalysts compared to the other studies.

In the high-frequency region, three peaks can be seen (Fig. 6b). The high-frequency peak correlated to the ORR shifts to higher frequencies

until a current density of 3.0 mA cm^{-2}, at which it shifts back. The frequency maximum of this ORR step is shifted to higher current densities compared to the CT of the ORR. However, no trend is evident in the corresponding impedance data. The impedance of the second high-frequency process exhibits a decrease with increasing current and an increase in frequency. The final peak assigned to the double-layer charging remains at 3177 Hz.

3.6. Koutecký-Levich vs. DRT analysis

Fig. 7 depicts the specific impedance contributions, as previously illustrated in Fig. 6c, as a share of the total impedance. The CT impedance at low current densities dominates the total cell impedance. As the current density increases, the share of the MT impedance rises gradually until it becomes the dominant impedance contribution. This observation follows the expected trend of RDE data such as linear sweep voltammograms (LSVs), which can be typically subdivided into three distinct regions: kinetic, mixed, and mass transport or diffusion-controlled region [27,28]. These regions are directly connected to the mathematical description of the Koutecký-Levich (KL) equation. Consequently, a common methodology for the determination of a catalyst's activity is the extraction of kinetic current information by applying the KL equation at a given potential [44]. The following section compares the theoretical description of the KL equation with the impedance shares obtained from the DRT analysis of the experimentally measured EIS data.

Fig. 8a displays the CT impedance share as determined from DRT in blue, while the theoretical curve of the current density divided by the kinetic current density is presented in black. In both cases, this should provide insight into the kinetic contribution at a given current density. The DRT values exhibit a linear relationship, with a coefficient of determination for the linear regression of over 98%. Nevertheless, a discrepancy between the two lines is evident, particularly at higher current densities. The DRT analysis is based on EIS data obtained at constant current. At these near-steady state conditions, the adsorption of hydroxide and/or the oxidation of the Pt surface occur over time [32,33, 45]. This observation can also be made in the experiment over time, as illustrated in Fig. 5. The rapid coverage of adsorbates (OH$_{ads}$ and O$_{ads}$) impedes the mass transport of oxygen to the electrode, particularly at higher current densities where the oxygen consumption is increased. This explains the decreased CT impedance share in that region compared to the ideal KL values. This interpretation is also confirmed by comparing the MT impedance share with the current density share of the limiting current density, as illustrated in Fig. 8b. The DRT data indicate an increased MT impedance share compared to the expected values based on the limiting current.

However, the data most commonly utilized in KL analysis are LSVs or CVs. In contrast to the EIS data, the data are acquired by scanning a potential, thereby rapidly altering the local environment at the electrode surface. Pt oxidation and hydroxide adsorption can be largely eliminated
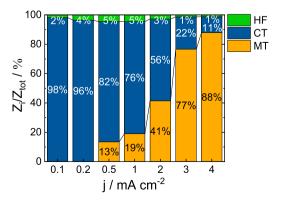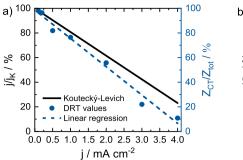

Fig. 7. Relative share of the impedance contribution relative to the total impedance based on the same data as in Fig. 6c.
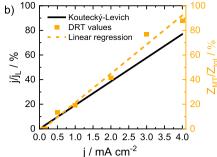
Fig. 8. a) Comparison of the CT impedance share derived from DRT and the current density share of the kinetic current density derived from the Koutecký-Levich equation, plotted over the current density; b) comparison between the MT impedance share derived from DRT and the current density share of the limiting current density, plotted over the current density.

by scanning to low potentials [46,47]. Accordingly, the data obtained from scanning are more closely aligned with the ideal KL relationship.

Although the KL evaluation is very suitable and widely used, it has some limitations. To ensure accurate results, the KL equation should be applied in a specific potential and current region, and a too-thick catalyst loading should be avoided [27,48,49]. Furthermore, a correct determination of the limiting current is essential when conducting KL [50]. However, in certain circumstances, it is not possible to establish a flat current plateau, making an identification of the limiting current challenging. The alternative evaluation approach, by linearizing one by the square root of the rotation rate against one by the measured current, is not always feasible. This is particularly the case when adsorbate effects in the kinetic region distort the order of dependence of the polarization curve on the rotation rate.

Moreover, KL cannot evaluate steady-state measurements at a constant current or constant potential over time. Consequently, long-term durability measurements for RDE are mainly performed as an accelerated stress test by cycling the electrode between a specified potential range [18,51]. However, other factors that may influence the durability of the catalyst, such as the adsorption of oxygenated species or Pt oxidation over time, can only be examined to a limited extent. This is because, as previously mentioned, the local environment changes during cycling. In this context, EIS measurements enable the possibility of performing in-situ steady-state measurements over time. When combined with DRT evaluation, they permit the extraction of specific contributions, including changes in the kinetic contribution.

4. Conclusion

This study performed EIS measurements on a Pt-RDE. The impedance spectra that were obtained were evaluated with DRT analysis. Individual parameters, such as the oxygen saturation level in the electrolyte, the rotation rate, and the current density, were varied, and their influence on the impedance contributions was examined. In the frequency range of 10^{-2}–10^4 Hz, four to five peaks were identified in the DRT plot. The two most prominent peaks are attributed to oxygen's mass transport (MT) impedance to the electrode and the ORR's charge transfer (CT) impedance. In addition, two to three minor high-frequency peaks were visible, which make up <5% of the total impedance in each experiment. These peaks were tentatively assigned to a side-step of the ORR, the adsorption of oxygenated species on the electrode, and the double-layer charging.

An increase in oxygen saturation level in the electrolyte results in a significant reduction in the MT impedance, whereas an increased rotation rate leads to an increase in the characteristic frequency of the MT and a slight rise in CT impedance. The measurement over time leads to a continuous increase in CT impedance caused by the adsorption of oxygenated species and by the place-exchange mechanism at the Pt surface. As the current density increases, a clear shift of the dominant impedance contribution from CT to MT impedance occurs. This finding

follows the Koutecký-Levich equation, which mathematically describes the hydrodynamic of the RDE. Due to the unique characteristics of the RDE, the presented peak assignment can serve as a guideline for other researchers employing DRT on RDE, even if they study a different reaction than the ORR. Furthermore, these findings can be used to develop and adapt equivalent circuit models for the RDE.

Finally, a direct correlation was observed between the CT impedance contribution extracted from the DRT and the theoretically expected kinetic current share based on Koutecký-Levich (KL). Therefore, EIS measurements in combination with DRT can be used as an alternative or complementary analysis tool for the typical KL evaluation, particularly for studies where the KL criteria are not fulfilled. This enables in-situ long-term steady-state measurements, with the possibility of monitoring changes in impedance contributions and their corresponding frequencies over time.

CRediT authorship contribution statement

Alexander Rampf: Writing – original draft, Methodology, Investigation, Formal analysis, Data curation, Conceptualization. **Carla Marchfelder:** Writing – review & editing, Methodology, Investigation. **Roswitha Zeis:** Writing – review & editing, Supervision, Project administration, Funding acquisition, Conceptualization.

Declaration of competing interest

The authors declare that they have no known competing financial interests or personal relationships that could have appeared to influence the work reported in this paper.

Acknowledgments

Supplementary materials

Supplementary material associated with this article can be found, in the online version, at doi:10.1016/j.electacta.2024.145583.

Data availability

Data will be made available on request.

References

[1] E. Ivers-Tiffée, A. Weber, Evaluation of electrochemical impedance spectra by the distribution of relaxation times, J. Ceram. Soc. Jpn. 125 (2017) 193–201, https://doi.org/10.2109/jcersj2.125.P4-1.

[2] M. Heinzmann, A. Weber, E. Ivers-Tiffée, Advanced impedance study of polymer electrolyte membrane single cells by means of distribution of relaxation times, J. Power Sources. 402 (2018) 24–33, https://doi.org/10.1016/j.jpowsour.2018.09.004.

[3] Y. Ao, Z. Li, S. Laghrouche, D. Depernet, D. Candusso, K. Zhao, Stack-level diagnosis of proton exchange membrane fuel cell by the distribution of relaxation times analysis of electrochemical impedance spectroscopy, J. Power Sources. 603 (2024), https://doi.org/10.1016/j.jpowsour.2024.234420.

[4] A. Weiß, S. Schindler, S. Galbiati, M.A. Danzer, R. Zeis, Distribution of relaxation times analysis of high-temperature PEM fuel cell impedance spectra, Electrochim. Acta 230 (2017) 391–398, https://doi.org/10.1016/j.electacta.2017.02.011.

[5] N. Bevilacqua, T. Asset, M.A. Schmid, H. Markötter, I. Manke, P. Atanassov, R. Zeis, Impact of catalyst layer morphology on the operation of high temperature PEM fuel cells, J. Power Sources Adv. 7 (2021) 100042, https://doi.org/10.1016/j.powera.2020.100042.

[6] M. Braig, R. Zeis, Distribution of relaxation times analysis of electrochemical hydrogen pump impedance spectra, J. Power. Sources. 576 (2023) 233203, https://doi.org/10.1016/j.jpowsour.2023.233203.

[7] Y. Li, Y. Jiang, J. Dang, X. Deng, B. Liu, J. Ma, F. Yang, M. Ouyang, X. Shen, Application of distribution of relaxation times method in polymer electrolyte membrane water electrolyzer, Chem. Eng. J. 451 (2023), https://doi.org/10.1016/j.cej.2022.138327.

[8] M. Schilling, M. Braig, K. Köble, R. Zeis, Investigating the V(IV)/V(V) electrode reaction in a vanadium redox flow battery – A distribution of relaxation times analysis, Electrochim. Acta 430 (2022) 141058, https://doi.org/10.1016/j.electacta.2022.141058.

[9] M. Schilling, R. Zeis, Investigating the V(II)/V(III) electrode reaction in a vanadium redox flow battery – A distribution of relaxation times analysis, Electrochim. Acta 477 (2024), https://doi.org/10.1016/j.electacta.2024.143771.

[10] A. Oz, S. Hershkovitz, N. Belman, E. Tal-Gutelmacher, Y. Tsur, Analysis of impedance spectroscopy of aqueous supercapacitors by evolutionary programming: finding DFRT from complex capacitance, Solid. State Ion. 288 (2016) 311–314, https://doi.org/10.1016/j.ssi.2015.11.008.

[11] T. Rüther, W. Hileman, G.L. Plett, M.S. Trimboli, M.A. Danzer, Demystifying the distribution of relaxation times: a simulation-based investigation into the limits and possibilities of interpretation for lithium-ion batteries, J. Electrochem. Soc. 171 (2024) 060508, https://doi.org/10.1149/1945-7111/ad4fe5.

[12] C. Plank, T. Rüther, L. Jahn, M. Schamel, J.P. Schmidt, F. Ciucci, M.A. Danzer, A review on the distribution of relaxation times analysis: a powerful tool for process identification of electrochemical systems, J. Power. Sources. 594 (2024) 233845, https://doi.org/10.5281/zenodo.8182851.

[13] T.H. Wan, M. Saccoccio, C. Chen, F. Ciucci, Influence of the discretization methods on the distribution of relaxation times deconvolution: implementing radial basis functions with DRTtools, Electrochim. Acta 184 (2015) 483–499, https://doi.org/10.1016/j.electacta.2015.09.097.

[14] A. Maradesa, B. Py, J. Huang, Y. Lu, P. Iurilli, A. Mrozinski, H.M. Law, Y. Wang, Z. Wang, J. Li, S. Xu, Q. Meyer, J. Liu, C. Brivio, A. Gavriluyk, K. Kobayashi, A. Bertei, N.J. Williams, C. Zhao, M. Danzer, M. Zic, P. Wu, V. Yrjänä, S. Pereverzyev, Y. Chen, A. Weber, S.V. Kalinin, J.P. Schmidt, Y. Tsur, B. A. Boukamp, Q. Zhang, M. Gaberšček, R. O'Hayre, F. Ciucci, Advancing electrochemical impedance analysis through innovations in the distribution of relaxation times method, Joule 8 (2024) 1958–1981, https://doi.org/10.1016/j.joule.2024.05.008.

[15] D. Zhu, T. Ma, Y. Yang, Optimization and application of the distribution of relaxation times based on characteristic frequency resolution and hyperparameters, J. Power. Sources 545 (2022), https://doi.org/10.1016/j.jpowsour.2022.231955.

[16] N. Schlüter, S. Ernst, U. Schröder, Finding the optimal regularization parameter in distribution of relaxation times analysis, ChemElectroChem. 6 (2019) 6027–6037, https://doi.org/10.1002/celc.201901863.

[17] S.S. Kocha, K. Shinozaki, J.W. Zack, D.J. Myers, N.N. Kariuki, T. Nowicki, V. Stamenkovic, Y. Kang, D. Li, D. Papageorgopoulos, Best practices and testing protocols for benchmarking ORR activities of fuel cell electrocatalysts using rotating disk electrode, Electrocatalysis 8 (2017) 366–374, https://doi.org/10.1007/s12678-017-0378-6.

[18] T. Nagai, J. Jahn, H. Jia, Improved accelerated stress tests for ORR catalysts using a rotating disk electrode, J. Electrochem. Soc. 166 (2019) F3111–F3115, https://doi.org/10.1149/2.0161907jes.

[19] N. Ramaswamy, S. Mukerjee, Fundamental mechanistic understanding of electrocatalysis of oxygen reduction on Pt and non-Pt surfaces: acid versus alkaline media, Adv. Phys. Chem. 491604 (2012) 1–17, https://doi.org/10.1155/2012/491604.

[20] X. Ge, A. Sumboja, D. Wuu, T. An, B. Li, F.W.T. Goh, T.S.A. Hor, Y. Zong, Z. Liu, Oxygen reduction in alkaline media: from mechanisms to recent advances of catalysts, ACS. Catal. 5 (2015) 4643–4667, https://doi.org/10.1021/acscatal.5b00524.

[21] M. Shao, Q. Chang, J.P. Dodelet, R. Chenitz, Recent advances in electrocatalysts for oxygen reduction reaction, Chem. Rev. 116 (2016) 3594–3657, https://doi.org/10.1021/acs.chemrev.5b00462.

[22] C.M. Pedersen, M. Escudero-Escribano, A. Velázquez-Palenzuela, L.H. Christensen, I. Chorkendorff, I.E.L. Stephens, Benchmarking Pt-based electrocatalysts for low

[23] Y. Sun, Y. Dai, Y. Liu, S. Chen, A rotating disk electrode study of the particle size effects of Pt for the hydrogen oxidation reaction, Phys. Chem. Chem. Phys. 14 (2012) 2278–2285, https://doi.org/10.1039/c2cp22761d.

[24] W. Sheng, H.A. Gasteiger, Y. Shao-Horn, Hydrogen oxidation and evolution reaction kinetics on platinum: acid vs alkaline electrolytes, J. Electrochem. Soc. 157 (2010) B1529, https://doi.org/10.1149/1.3483106.

[25] M.F. Tesch, S. Neugebauer, P.V. Narangoda, R. Schlögl, A.K. Mechler, The rotating disc electrode: measurement protocols and reproducibility in the evaluation of catalysts for the oxygen evolution reaction, Energy Adv. 2 (2023) 1823–1830, https://doi.org/10.1039/d3ya00340j.

[26] A.H.M. da Silva, R.E. Vos, R.J.C. Schrama, M.T.M. Koper, Design of a Rotating Disk Electrode setup operating under high pressure and temperature: application to CO2 reduction on gold, Electrochim. Acta 498 (2024), https://doi.org/10.1016/j.electacta.2024.144612.

[27] W. Chen, Q. Xiang, T. Peng, C. Song, W. Shang, T. Deng, J. Wu, Reconsidering the benchmarking evaluation of catalytic activity in oxygen reduction reaction, iScience 23 (2020) 101532, https://doi.org/10.1016/j.isci.

[28] J. Wang, C.X. Zhao, J.N. Liu, D. Ren, B.Q. Li, J.Q. Huang, Q. Zhang, Quantitative kinetic analysis on oxygen reduction reaction: a perspective, Nano Mater. Sci. 3 (2021) 313–318, https://doi.org/10.1016/j.nanoms.2021.03.006.

[29] M. Schönleber, D. Klotz, E. Ivers-Tiffée, A method for improving the robustness of linear Kramers-Kronig validity tests, Electrochim. Acta 131 (2014) 20–27, https://doi.org/10.1016/j.electacta.2014.01.034.

[30] A.C. Lazanas, M.I. Prodromidis, Electrochemical impedance spectroscopy-a tutorial, ACS. Meas. Sci. Au 3 (2023) 162–193, https://doi.org/10.1021/acsmeasuresciau.2c00070.

[31] N. Bevilacqua, M.A. Schmid, R. Zeis, Understanding the role of the anode on the polarization losses in high-temperature polymer electrolyte membrane fuel cells using the distribution of relaxation times analysis, J. Power. Sources. 471 (2020) 228469, https://doi.org/10.1016/j.jpowsour.2020.228469.

[32] N.M. Markovic, H.A. Gasteiger, P.N. Ross, Oxygen reduction on platinum low-index single-crystal surfaces in alkaline solution: rotating ring disk Pt(hkl) studies, J. Phys. Chem. 100 (1996) 6715–6721. https://pubs.acs.org/sharingguidelines.

[33] G.K.H. Wiberg, M. Arenz, Establishing the potential dependent equilibrium oxide coverage on platinum in alkaline solution and its influence on the oxygen reduction, J. Power Sources. 217 (2012) 262–267, https://doi.org/10.1016/j.jpowsour.2012.06.019.

[34] A.A. Moya, Identification of characteristic time constants in the initial dynamic response of electric double layer capacitors from high-frequency electrochemical impedance, J. Power Sources. 397 (2018) 124–133, https://doi.org/10.1016/j.jpowsour.2018.07.015.

[35] E. Santos, W. Schmickler, On the timescale of electrochemical processes, Electrochim. Acta 498 (2024), https://doi.org/10.1016/j.electacta.2024.144659.

[36] A. Rampf, M. Braig, S. Passerini, R. Zeis, A comparative study of the oxygen reduction reaction on pt and ag in alkaline media, ChemElectroChem (2024), https://doi.org/10.1002/celc.202400563.

[37] R.K. Singh, R. Devivaraprasad, T. Kar, A. Chakraborty, M. Neergat, Electrochemical impedance spectroscopy of oxygen reduction reaction (ORR) in a rotating disk electrode configuration: effect of ionomer content and carbon-support, J. Electrochem. Soc. 162 (2015) F489–F498, https://doi.org/10.1149/2.0141506jes.

[38] K. Shinozaki, J.W. Zack, S. Pylypenko, B.S. Pivovar, S.S. Kocha, Oxygen reduction reaction measurements on platinum electrocatalysts utilizing rotating disk electrode technique, J. Electrochem. Soc. 162 (2015) F1384–F1396, https://doi.org/10.1149/2.0551512jes.

[39] A. Kongkanand, J.M. Ziegelbauer, Surface platinum electrooxidation in the presence of oxygen, J. Phys. Chem. C 116 (2012) 3684–3693, https://doi.org/10.1021/jp211490a.

[40] M. Matsumoto, T. Miyazaki, H. Imai, Oxygen-enhanced dissolution of platinum in acidic electrochemical environments, J. Phys. Chem. C 115 (2011) 11163–11169, https://doi.org/10.1021/jp201959h.

[41] B. Ruiz-Camacho, J.C. Baltazar Vera, A. Medina-Ramírez, R. Fuentes-Ramírez, G. Carreño-Aguilera, EIS analysis of oxygen reduction reaction of Pt supported on different substrates, Int. J. Hydrogen. Energy 42 (2017) 30364–30373, https://doi.org/10.1016/j.ijhydene.2017.08.087.

[42] J. Perez, E.R. Gonzalez, E.A. Ticianelli, Oxygen electrocatalysis on thin porous coating rotating platinum electrodes, Electrochim. Acta 44 (1998) 1329–1339, https://doi.org/10.1016/S0013-4686(98)00255-2.

[43] J. Perez, E.R. Gonzalez, E.A. Ticianelli, Impedance studies of the oxygen reduction on thin porous coating rotating platinum electrodes, J. Electrochem. Soc 145 (1998), https://doi.org/10.1149/1.1838635.

[44] K. Shinozaki, J.W. Zack, S. Pylypenko, R.M. Richards, B.S. Pivovar, S.S. Kocha, Benchmarking the oxygen reduction reaction activity of Pt-based catalysts using standardized rotating disk electrode methods, Int. J. Hydrogen. Energy 40 (2015) 16820–16830, https://doi.org/10.1016/j.ijhydene.2015.08.024.

[45] N.P. Subramanian, T.A. Greszler, J. Zhang, W. Gu, R. Makharia, Pt-oxide coverage-dependent oxygen reduction reaction (ORR) kinetics, J. Electrochem. Soc. 159 (2012) B531–B540, https://doi.org/10.1149/2.088205jes.

[46] Y. Zhang, S. Chen, Y. Wang, W. Ding, R. Wu, L. Li, X. Qi, Z. Wei, Study of the degradation mechanisms of carbon-supported platinum fuel cells catalyst via different accelerated stress test, J. Power Sources 273 (2015) 62–69, https://doi.org/10.1016/j.jpowsour.2014.09.012.

[47] M. Waje, W. Li, Z. Chen, P. Larsen, Y. Yan, Effect of scan range on Pt surface area loss in potential cycling experiments, ECS. Trans. 11 (2007) 1227–1233, https://doi.org/10.1149/1.2781036.

[48] S. Xu, Y. Kim, D. Higgins, M. Yusuf, T.F. Jaramillo, F.B. Prinz, Building upon the Koutecky-Levich equation for evaluation of next-generation oxygen reduction reaction catalysts, Electrochim. Acta 255 (2017) 99–108, https://doi.org/10.1016/j.electacta.2017.09.145.

[49] F.J. Vidal-Iglesias, J. Solla-Gullón, V. Montiel, A. Aldaz, Errors in the use of the Koutecky-Levich plots, Electrochem. Commun. 15 (2012) 42–45, https://doi.org/10.1016/j.elecom.2011.11.017.

[50] W. Chen, H.W. Cui, L.W. Liao, Y.J. Xu, J. Cai, Y.X. Chen, Challenges in unravelling the intrinsic kinetics of gas reactions at rotating disk electrodes by Koutecky-Levich equation, J. Phys. Chem. C 127 (2023) 16235–16248, https://doi.org/10.1021/acs.jpcc.3c02677.

[51] S. Zaman, A.I. Douka, L. Noureen, X. Tian, Z. Ajmal, H. Wang, Oxygen reduction performance measurements: discrepancies against benchmarks, Battery Energy 2 (2023), https://doi.org/10.1002/bte2.20220060.